

Deferoxamine Treatment Effectively Prevents Periodontitis Progression by Reducing Inflammation and Osteoclastogenesis in Experimental Periodontitis Rats

Yanlin Zhu^{1,2}, Shuwei Qiao^{2,3}, Yuxuan Pang^{2,3}, Huimin Wang^{2,3}, Yanmin Zhou^{1,2}

¹Department of Dental Implantology, Hospital of Stomatology, Jilin University, Changchun, People's Republic of China; ²Jilin Provincial Key Laboratory of Tooth Development and Bone Remodeling, Hospital of Stomatology, Jilin University, Changchun, People's Republic of China; ³Department of Prosthodontics, Hospital of Stomatology, Jilin University, Changchun, People's Republic of China

Correspondence: Yanmin Zhou, Jilin Provincial Key Laboratory of Tooth Development and Bone Remodeling, Hospital of Stomatology, Jilin University, 1500 Qinghua Road, Changchun, Jilin Province, 130021, People's Republic of China, Tel +8618943971001, Email zhouym@jlu.edu.cn

Purpose: Although the anti-inflammatory properties of the hypoxia-mimetic drug deferoxamine (DFO) have been reported, its potential as a treatment for periodontitis remains unknown. This study investigated the therapeutic benefits of DFO on osteoclastogenesis and inflammation in periodontitis progression.

Methods: RAW264.7 cells were pretreated with DFO before stimulation with lipopolysaccharides from *Porphyromonas gingivalis* (*P.g*-LPS). Hypoxia-inducible factor-1 α (HIF-1 α) and inflammatory factors were measured, followed by analysis of relevant inflammatory pathways. Immunofluorescence and molecular biology methods were employed to assess osteoclast differentiation in RAW264.7 cells after nuclear factor- κ B ligand (RANKL) induction. A rat model of periodontitis was established using ligature wires, and alveolar bone loss was assessed via micro-computed tomography. Osteoclastogenesis and periodontal inflammation were assessed through immunohistochemistry as well as hematoxylin and eosin staining.

Results: DFO reduced the *P.g*-LPS-induced inflammatory factor expression ($P < 0.0001$) and upregulated HIF-1 α ($P = 0.0278$) in RAW264.7 cells. DFO suppressed NF- κ B signaling by inhibiting NF- κ B p65 nuclear translocation and phosphorylation. DFO pretreatment inhibited osteoclast development by decreasing F-actin rings synthesis, reducing the number of mature osteoclasts ($P < 0.0001$) and downregulating osteoclast-specific markers ($P < 0.05$). In rat periodontitis models, DFO treatment reduced tissue inflammation, osteoclastogenesis, and alveolar bone loss ($P < 0.05$).

Conclusion: DFO effectively prevented osteoclast development, alveolar bone loss, and inflammation associated with periodontitis.

Keywords: deferoxamine, periodontitis, inflammation, osteoclast differentiation

Introduction

Bacterial plaque, a collection of bacteria, is the primary factor in periodontitis, an inflammatory disease caused by bacterial infection that leads to bone loss in periodontal supporting tissues. *Porphyromonas gingivalis* (*P.g*) is one of the primary pathogens involved in the initiation and progression of periodontitis.¹ The lipopolysaccharide derived from *P.g* (*P.g*-LPS) either directly damages tissue or indirectly induces inflammation by activating other mediators.² *P.g*-LPS binds to Toll-like receptors on macrophages activating them and stimulating the nuclear factor- κ B (NF- κ B) pathway, a key mediator in periodontitis.³ This activation leads to the overproduction of proinflammatory cytokines, including interleukin-6 (IL-6), tumor necrosis factor- α (TNF- α), and interleukin-1 β (IL-1 β),⁴ which contribute to alveolar bone resorption and connective tissue damage.⁵

Chronic inflammation often leads to regional hypoxia because activated immune cells and inflamed tissues consume local oxygen supplies more rapidly.² Under hypoxic conditions, hypoxia-inducible factors (HIFs) play a crucial role in maintaining cellular homeostasis. The HIF-1 transcription factor, composed of an oxygen-regulated alpha subunit and

a beta subunit, is especially important in this process. Under hypoxic conditions, HIF-1 α is stabilised and pairs with HIF-1 β in the nucleus to form the active HIF-1 complex, which binds to hypoxia-responsive elements to initiate the expression of downstream genes that respond to the hypoxic environment.⁶

HIF-1 α directly regulates the survival and function of macrophages within inflammatory environments. Under hypoxic environments, HIF-1 α suppresses oxidative phosphorylation, shifting ATP production to glycolysis.⁷ It also regulates glycolytic enzymes, thus facilitating the conversion of energy metabolism sources for macrophages.⁸ At normoxic oxygen levels, the HIF prolyl hydroxylase (PHD) domain protein uses oxygen and α -ketoglutarate as substrates to modify HIF-1 α by hydroxylating two proline residues. Hydroxylated HIF-1 α undergoes rapid degradation by the Von Hippel-Lindau protein, suppressing HIF-1 α -mediated gene transcription.⁹

The United States Food and Drug Administration has approved deferoxamine (DFO), a hypoxia-mimetic agent, as an iron-chelating drug.^{10,11} By chelating Fe²⁺ at the catalytic site of PHD proteins, DFO activates of the hypoxic HIF-1 α pathway enhancing both the immune response and glycolytic activity in macrophages.^{12,13} Numerous studies indicate that PHD inhibitors have potential anti-inflammatory effects^{2,14,15} including modulating T-cell differentiation, cytotoxic activity, and the microbicidal capacity of phagocytes through HIF activation.¹⁶ Furthermore, PHD inhibition generally downregulates the NF- κ B pathway¹⁷ highlighting the HIF/PHD pathway as a promising target for inflammatory disease treatment.

DFO downregulate the activation of mitogen-activated protein kinases while also suppressing the electron transport chain, thereby preventing osteoclast differentiation.¹⁸ By stabilizing HIF-1 α , DFO prevents its degradation, promoting neovascularization, and further inhibits osteoclastogenesis while synergizing with osteoinductive scaffolds to facilitate bone regeneration.¹⁹

While DFO's anti-inflammatory properties are well established, its use in the oral cavity remains largely unexplored. Despite the similarities in immune responses to inflammation, the unique environment of the mouth, with its distinct microbiome and constant exposure to external stimuli, raises questions about DFO's efficacy and safety in this specific context. Therefore, research exploring the potential benefits and challenges of DFO application in the oral cavity is crucial. The objective of our study was to assess DFO's efficacy and safety in a rat model of periodontitis. The first experimental hypothesis was that DFO treatment failed to reduce the damaging effects of periodontitis. The second experimental hypothesis was that DFO had no connection with inhibitory effects on the proinflammatory signaling pathways.

Materials and Methods

Cells and Treatments

Mouse leukemia cells of monocyte macrophage (RAW264.7 cells) from Procell Life Science & Technology (Wuhan, China) were cultured in high-glucose dulbecco's modified Eagle medium (HG-DMEM) (Gibco, NY, USA) to which 10% fetal bovine serum (FBS) (Gibco, NY, USA) had been added in a 37 °C incubator with 5% CO₂. Cells were treated with DFO (Sigma-Aldrich, St. Louis, MO, USA) at concentrations of 0, 12.5, 20, 50, or 100 μ M for 2 hours, after which *P.g*-LPS (1 μ g/mL, InvivoGen, Toulouse, France) was added. Cells were incubated for another 22 hours at 37 °C before further experiments.

Cell Viability Assay

RAW264.7 cells were treated with varying concentrations of DFO (Sigma-Aldrich, St Louis, MO, USA) for 24 hours. Post-treatment, the medium was replaced with 100 μ L of 10% CCK-8 solution (Beyotime, Shanghai, China), and cells were incubated at 37 °C, shielded from direct light. Absorbance at 450 nm was measured using a microplate reader (Bole Life Medical Products, Shanghai, China) to assess cell viability.

Real Time-Quantitative Polymerase Chain Reaction (RT-qPCR)

Total RNA was isolated and purified using the MolPure TRleasy Plus Total RNA Kit (YEASEN, Shanghai, China) following the manufacturer's protocol. Reverse transcription was performed using the Hifair III 1st Strand cDNA Synthesis SuperMix for qPCR (gDNA digester plus) (YEASEN, Shanghai, China). RT-qPCR was carried out with the Hieff qPCR SYBR Green Master Mix (YEASEN, Shanghai, China) on a CFX96 RT-qPCR Detection System (Bio-Rad, CA, USA). Amplification conditions included an initial denaturation at 95 °C for 10 minutes, followed by 40 cycles of 95 °C for 10 seconds and 60 °C for 30 seconds.

Table 1 The Primer Sequences for RT-qPCR

Gene (murine)	Forward Primer (5'-3')	Reverse Primer (5'-3')
IL-1 β	TCCAGGATGAGGACATGAGCAC	GAACGTCACACACCAGCAGGTTA
IL-6	CCGGAGAGGAGACTTCACAG	CAGAATTGCCATTGCACAAC
TNF- α	TATGGCCAGACCCTCACAC	GGAGTAGACAAGGTACAACCCATC
HIF-1 α	AGCTTGCTCATCAGTTGCCA	CCAGAAGTTTCTCACACGC
NFATc1	CCCGTCACATTCTGGTCCAT	CAAGTAACCGTGTAGCTGCACA
TRAP	CAAGAACTTGCGACCATTGTTA	ATCCATAGTGAAACCGCAAGTA
CTSK	CACCCAGTGGGAGCTATGGAA	GCCTCCAGGTTATGGGCAGA
Beta Actin	GGAGATTACTGCCCTGGCTCCTA	GGAGTAGACAAGGTACAACCCATC

Abbreviations: IL 6, interleukin 6; CTSK, cathepsin K; HIF-1 α , hypoxia-inducible factor 1 alpha; TRAP, gene encoding tartrate-resistant acid phosphatase; TNF- α , tumor necrosis factor- α ; NFATc1, nuclear factor of activated T-cells cytoplasmic 1; IL 1 β , interleukin 1 beta.

Relative mRNA expression levels were calculated using the $2^{-\Delta\Delta Ct}$ method. Primer sequences used for RT-qPCR are listed in Table 1.

Western Blotting

Cell lysis was performed using a radioimmunoprecipitation assay buffer (Beyotime, Shanghai, China) with a phosphatase inhibitor and 1 mm of phenylmethanesulfonyl fluoride (Beyotime, Shanghai, China). Lysates were then centrifuged at 12,000 \times g for 15 minutes at 4 $^{\circ}$ C. Loading buffer (Beyotime, Shanghai, China) was mixed with the resulting supernatant and incubated for 5 minutes at 100 $^{\circ}$ C before storing the protein samples at -20 $^{\circ}$ C until required. Protein concentrations were determined using the bicinchoninic acid method, followed by separation using SDS-polyacrylamide gel electrophoresis (Bio-Rad, CA, USA). Proteins were transferred to nitrocellulose membranes using the wet transfer method, and membranes were blocked for 15 minutes with QuickBlock Blocking Buffer (Beyotime, Shanghai, China). Membranes were then incubated overnight at 4 $^{\circ}$ C with primary antibodies including: rabbit anti-IL-1 β (1:1000, ab254360), rabbit anti-IL-6 (1:1000, ab290735), rabbit anti-HIF-1 α (1:1000, ab179483), rabbit anti-IK β (1:1000, ab32518), rabbit anti-TNF- α (1:1000, ab205587) from Abcam (Cambridge, England). Phospho-NF- κ B p65 (Ser536) peptide (1:1000, AF2006-BP) from Affinity Biosciences (Cincinnati, OH, USA), rabbit anti-NF- κ B p65 (1:1000, #8242, Cell Signaling Technology, Danvers, MA, USA) and mouse anti- β -actin (1:1000, 66,009-1-Ig, Proteintech, Chicago, USA). Membranes were washed and incubated for 1 hour with Horseradish Peroxidase (HRP)-conjugated secondary antibodies: HRP-labeled Goat Anti-Mouse IgG (H+L) antibody (1:1000, A0216, Beyotime, Shanghai, China) and HRP-labeled Goat Anti-Rabbit IgG (H+L) antibody (1:1000, A0208, Beyotime, Shanghai, China). Finally, the protein bands were visualized using enhanced chemiluminescence (1:1000, NCM Biotech, Suzhou, China) and quantified with Image J software (version 1.53e, USA).

Immunofluorescence Detection of p65 Nucleation in Cells

Cell slides were fixed in 4% paraformaldehyde for 15 minutes. Slides were washed thrice with phosphate-buffered saline for 5 minutes each to remove residual fixative. Cells were permeabilized with 0.1% Triton X-100 (Beyotime, Shanghai, China), followed by overnight incubation at 4 $^{\circ}$ C with the primary antibody against p65 (Cell Signaling Technology, Boston, USA). The following day, cells were washed and incubated for 1 hour at room temperature in the dark with Cy3-labeled secondary antibody IgG (Invitrogen, Carlsbad, CA, USA). Nuclei were stained with 4,6-diamino-2-phenylindole (DAPI) (Beyotime, Shanghai, China). Images were captured using a 200 \times fluorescence microscope (Olympus, Tokyo, Japan).

Tartrate-Resistant Acid Phosphatase (TRAP) Staining

RAW264.7 cells, cultured in HG-DMEM, were treated for 2 hours with 12.5, 25, or 50 μ m of DFO. The HG-DMEM was replaced with Minimum Essential Medium Alpha (Gibco, NY, USA) containing 50 ng/mL of RANKL (PeproTech, MA, USA) and 10% FBS. Osteoclast development was evaluated using a TRAP/alkaline phosphatase (ALP) staining kit (WAKO, Osaka, Japan).

Fibrous Actin (F-Actin) Staining

RAW264.7 cells treated with RANKL were fixed using 4% paraformaldehyde (Beyotime, Shanghai, China) and permeabilized with 0.1% Triton X-100 (Beyotime, Shanghai, China). After washing, the cells were stained with TRITC-conjugated phalloidin (1:100 dilution; Solarbio, Beijing, China) to visualize actin ring formation. Nuclei were counterstained with DAPI (Beyotime, Shanghai, China) before imaging. F-actin rings were observed under fluorescence microscopy (OLYMPUS FLOUVIEW FV3000, Tokyo, Japan), and images were analyzed to quantify the number and size of actin rings in RANKL-induced cells.

Establishment of the Rat Periodontitis Model

Thirty-six male Sprague-Dawley rats (6-weeks old; 200–250 g) were maintained in a controlled environment, with specific pathogen-free conditions, regulated temperature (25 ± 2 °C), and a consistent light/dark cycle (12 hours). They had access to a standard rodent diet and water at all times. The rats were randomly assigned to three groups ($n = 12$ per group): (i) periodontitis group (PG), (ii) DFO treatment group (DG), (iii) blank control (BC). Rats were anesthetized with an intraperitoneal injection of 4 mL/kg pentobarbital sodium (1%) (Beyotime, Shanghai, China). A 0.2 mm-diameter orthodontic wire was then placed between the left maxillary first and second molars of each experimental rat. In the PG and DG groups, the wires were secured around the first molar. No ligature wires were used in the BC group. The PG group received was injected with saline at the affected site every other day, while the DG group received 100 μ L of DFO solution (200 μ M in saline). The reagent was injected into the gingival papilla, specifically at the buccal and palatal alveolar ridge crest between the first and second molars on the right side of the maxillary jaw. After three weeks, all rats were euthanized for analysis.

Micro-Computed Tomography (Micro-CT) Evaluation

Maxillae from each rat were collected and preserved in 4% paraformaldehyde. Alveolar bone loss was assessed using micro-CT imaging (SkyScan1172, 400 ms, 100 μ A, 83 kV) (Bruker, German). Scanned data were reconstructed with NRecon software (version 1.6.10.1, Bruker, German) and analyzed using CTan and CTvox software (Bruker, German). The extent of alveolar bone loss was measured by calculating the distance between the cemento-enamel junction (CEJ) and the alveolar bone crest (ABC) at six locations on the first molar: proximal, middle, and distal on both the buccal and palatal surfaces. Additionally, the bone mineral density (BMD) and bone volume/tissue volume (BV/TV) ratios were calculated to assess alveolar bone mass between the first and second molars.

Histological Analysis

Samples were dehydrated, embedded, and sectioned for histological evaluation. Hematoxylin and eosin (H&E) staining was performed to detect tissue inflammation, and immunohistochemistry (IHC) was used to assess levels of cathepsin K (CTSK), TRAP, IL-6, TNF- α , and IL-1 β in periodontitis-affected regions. Key organs (kidneys, spleen, lungs, heart, and liver) were also dissected, fixed in formalin, sectioned, and stained with H&E for toxicity assessment of DFO in vivo. All the experimental procedures were performed by the same operator in order to reduce random errors.

Statistical Analyses

Data processing was undertaken with GraphPad Prism 8 software (La Jolla, CA, USA). All data are presented as mean \pm standard deviation (SD). For independent samples, a two-tailed Student's *t*-test was used for two-group comparisons, while multiple groups were compared with one-way analysis of variance (ANOVA) followed by Tukey's post-hoc test for pairwise comparisons. Statistical significance was defined as *P* value of < 0.05 .

Results

Effects of DFO on RAW264.7 Cell Viability

Cell viability decreased by 13.76% at 100 μ M and showed a more significant reduction at 200 μ M ($P = 0.0166$), suggesting increased cytotoxicity at higher DFO concentrations (Figure 1A). Based on these results, doses of 12.5, 25, and 50 μ M were selected for further 24-hour experiments.

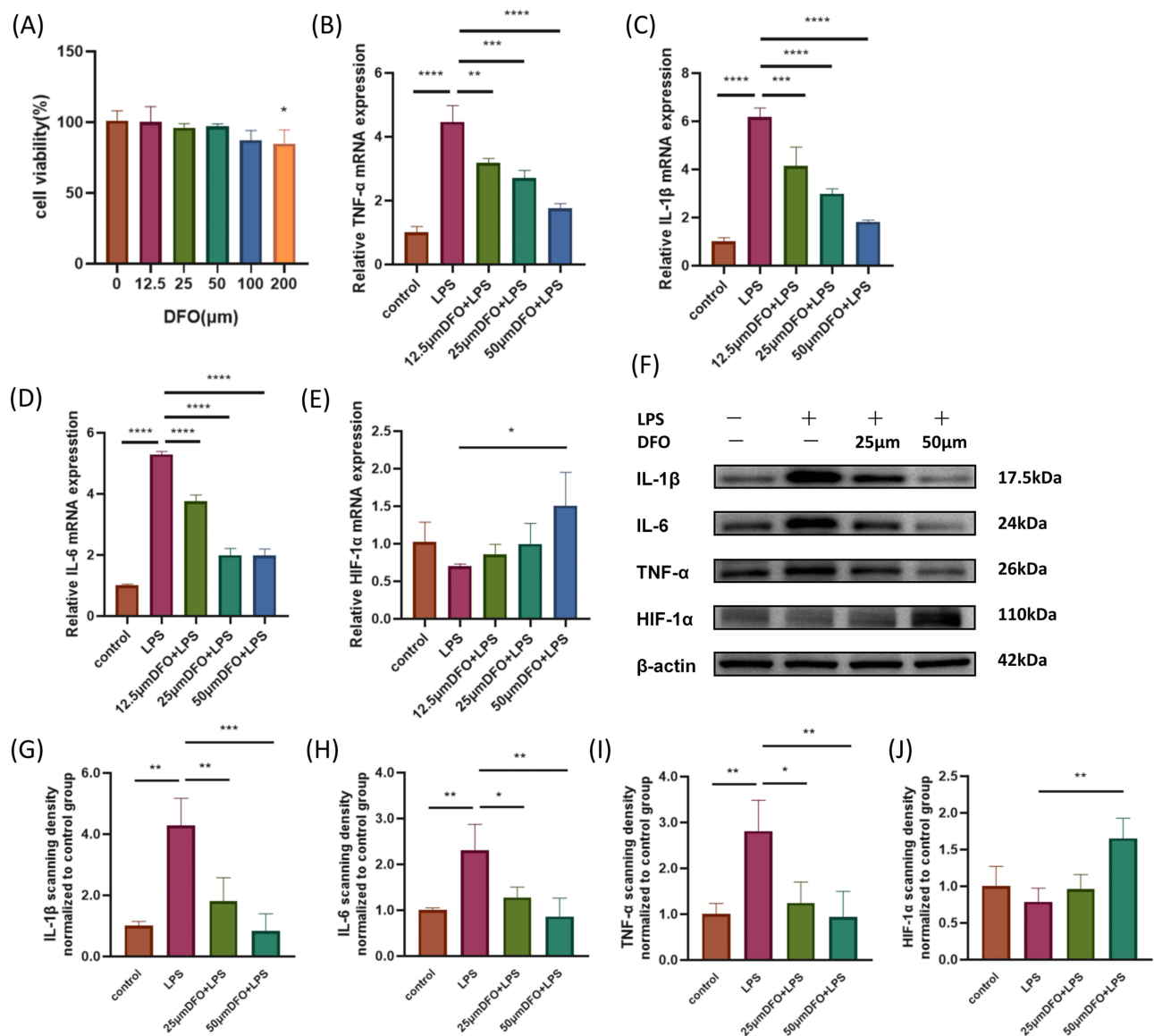


Figure 1 DFO reduces inflammation and upregulates HIF-1 α expression in RAW264.7 cells. **(A)** RAW264.7 cells were treated with varying DFO concentrations for 24 hours, and cell viability was assessed using the CCK-8 assay. **(B-E)** mRNA levels of TNF- α , IL-1 β , IL-6, and HIF-1 α after 24-hour treatment with *P.g*-LPS and DFO in RAW264.7 cells. **(F)** Protein expression levels of TNF- α , IL-1 β , IL-6, and HIF-1 α after 24-hour *P.g*-LPS and DFO treatment. Band intensities for **(G)** IL-1 β , **(H)** IL-6, **(I)** TNF- α , and **(J)** HIF-1 α were quantified and expressed as fold change relative to the control * $P < 0.05$, ** $P < 0.01$, *** $P < 0.001$, and **** $P < 0.0001$.

DFO Reduced Inflammation and Increases HIF-1 α Expression in RAW264.7 Cells

The anti-inflammatory effects of DFO in RAW264.7 cells were examined using RT-qPCR and Western blotting. Following *P.g*-LPS stimulation, TNF- α (Figure 1B, $P < 0.0001$), IL-1 β (Figure 1C, $P < 0.0001$), and IL-6 (Figure 1D, $P < 0.0001$) levels were significantly elevated. DFO treatment significantly reduced these inflammatory markers, with the 50 μ M dose showing the strongest inhibition ($P < 0.0001$). Moreover, DFO increased HIF-1 α expression under normoxic conditions, with the 50 μ M dose yielding significantly higher HIF-1 α levels compared to the *P.g*-LPS group (Figure 1E, $P = 0.0278$).

Similarly, Western blot analysis of RAW264.7 cells (Figure 1F) revealed increased levels of IL-1 β (Figure 1G, $P = 0.0001$), IL-6 (Figure 1H, $P = 0.0039$), and TNF- α (Figure 1I, $P < 0.0001$) proteins in the *P.g*-LPS group compared to the control group. The 50 μ M DFO treatment significantly attenuated these elevations (IL-1 β : Figure 1G, $P = 0.0002$) (IL-6: Figure 1H, $P = 0.0036$) (TNF- α : Figure 1I, $P < 0.0001$) and improved HIF-1 α protein level (Figure 1J, $P = 0.0022$). The consistency between Western

blot and RT-qPCR data demonstrated that DFO not only mitigated the *P.g*-LPS-induced inflammatory but also upregulated HIF-1 α expression.

DFO Inhibits NF- κ B Activation in *P.g*-LPS-Induced RAW264.7 Cells

Western blotting was used to quantify total I κ B α , phosphorylated I κ B α (p-I κ B α), total p65 and phosphorylated p65 (p-p65) (Figure 2A), key markers within the NF- κ B signaling cascade. Overall, the *P.g*-LPS group had lower I κ B α protein level (Figure 2B, $P = 0.0014$), higher p-p65 (Figure 2C, $P < 0.0001$) and p-I κ B α levels (Figure 2D, $P < 0.0001$) in comparison with the control, whereas DFO treatment dose-dependently increased I κ B α level (Figure 2B, $P < 0.01$), lowered the p-p65 (Figure 2C, $P < 0.0001$) and p-I κ B α levels (Figure 2D, $P < 0.0001$) in *P.g*-LPS-stimulated RAW264.7 cells. However, total p65 levels remained unchanged (Figure 2E). These findings indicate that DFO effectively inhibits *P.g*-LPS-mediated activation of NF- κ B signaling, resulting in reduced inflammatory responses in macrophages.

DFO Reduces p65 Nuclear Translocation to Suppress NF- κ B Activation

The nuclear translocation of p65, a key component of NF- κ B signaling, indicates its activation. Immunofluorescence staining was used to visualize p65 nuclear translocation, an important step in NF- κ B pathway activation. Treatment with 50 μ M DFO significantly decreased the nuclear fluorescence intensity of p65 (Figure 3), suggesting that DFO inhibits p65 nuclear translocation, thereby blocking NF- κ B activation and reducing downstream inflammatory responses.

DFO Inhibits Osteoclast Development in RANKL-Stimulated RAW264.7 Cells

In the TRAP staining assay, TRAP enzyme activity resulted in red or brown deposits, indicating osteoclasts (Figure 4A). The 50 μ M DFO significantly inhibited RANKL-induced osteoclast differentiation, as indicated by fewer TRAP-positive

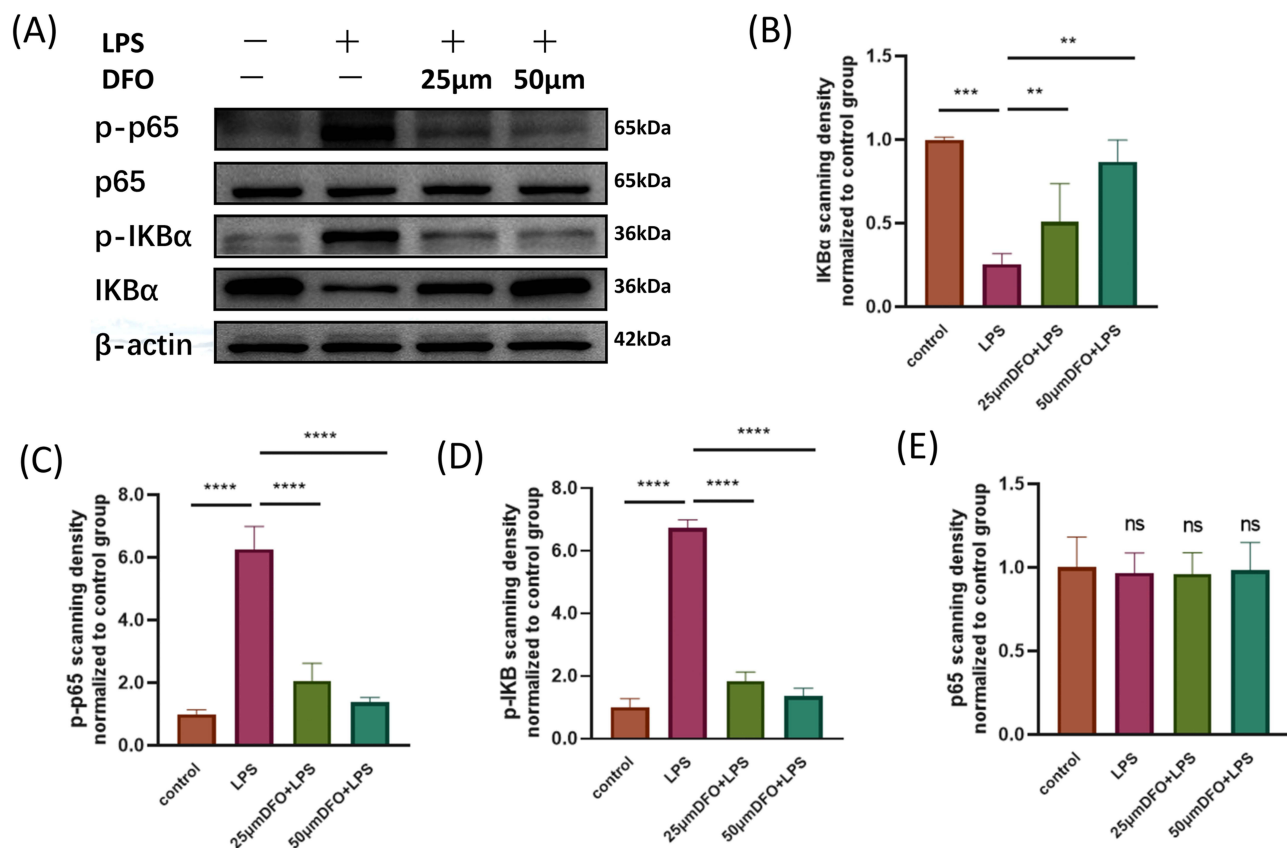


Figure 2 DFO suppresses NF- κ B activation in *P.g*-LPS-induced inflammation in RAW264.7 cells. (A) Protein expression levels of p-p65, p65, p-I κ B α , and I κ B α after 24-hour treatment with *P.g*-LPS and DFO. Band intensities for (B) I κ B α , (C) p-p65, (D) p-I κ B α , and (E) p65 were quantified and expressed as fold change relative to the control. ** $P < 0.01$, *** $P < 0.001$, **** $P < 0.0001$, ns: not significant.

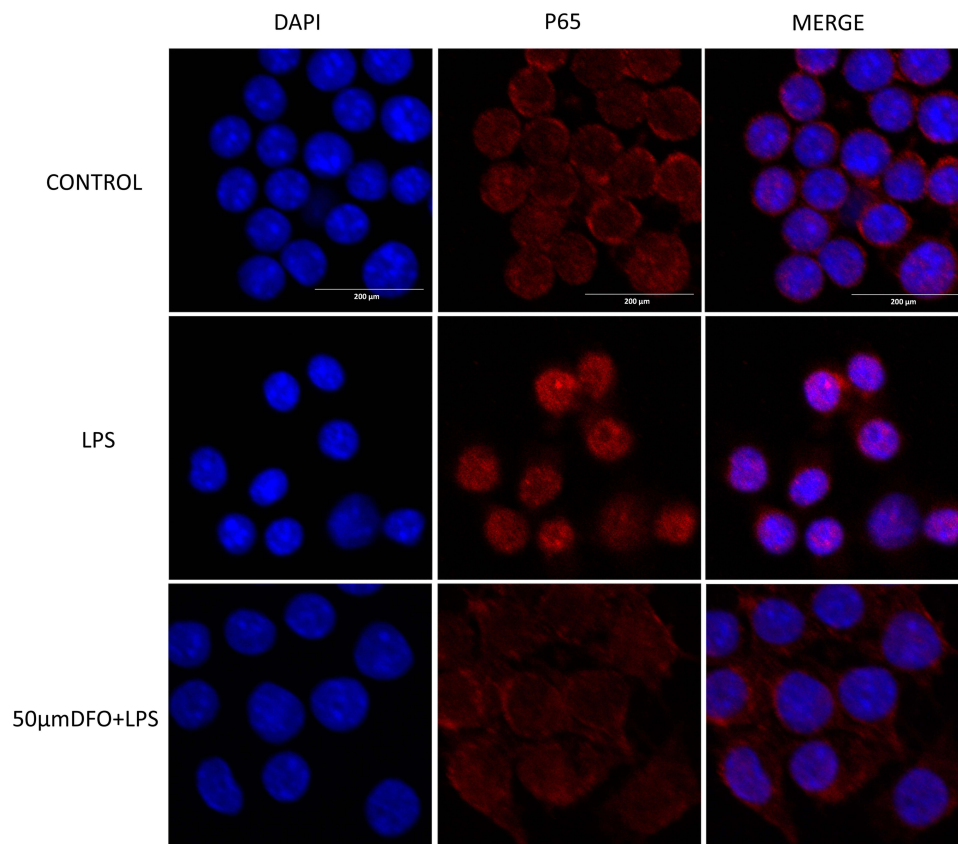


Figure 3 P65 nuclear translocation assessed by immunofluorescence staining; scale bar = 200 μ m.

cells (nuclei/cell ≥ 3) and the smaller osteoclasts (Figure 4B, $P < 0.0001$). Furthermore, RT-qPCR analysis of RANKL-stimulated cells showed significant downregulation in TRAP ($P = 0.0014$), cathepsin K (CTSK) ($P = 0.0129$) and nuclear factor of activated T-cells cytoplasmic 1 (NFATc1) ($P = 0.0020$) expression following pretreatment with 50 μ M DFO (Figure 4C), confirming its role in inhibiting osteoclast differentiation. Immunofluorescence staining of F-actin revealed a reduction in F-actin ring formation, which reflects osteoclast morphology, size, and structure. This decrease in F-actin rings corroborated the TRAP staining results, indicating fewer and smaller osteoclasts (Figure 4D). These findings suggest that DFO effectively modulates osteoclast number and morphology.

DFO Treatment Reduces Periodontal Inflammation and Alveolar Bone Loss

After euthanizing the rats, histological analysis of the maxillae and major organs was conducted. No histological abnormalities were observed in any group upon H&E staining of major organs, including the kidneys, lungs, spleen, heart, and liver (supplementary materials), highlighting the biosafety of localized DFO injections.

Micro-CT analysis showed that rats in the PG experienced significant alveolar bone resorption, which was attenuated in the DG (Figure 5A). The DG group displayed higher BV/TV (Figure 5B, $P = 0.005$) and BMD (Figure 5C, $P = 0.034$) compared to the PG group. Moreover, the CEJ to ABC distance was greater in the PG group than in the BC (Figure 5D, $P < 0.0001$) and DG groups (Figure 5D, $P = 0.016$).

Histological examination of the periodontal tissues from the PG revealed significant inflammatory cell infiltration, which was notably reduced following DFO treatment (Figure 5E). IHC staining (Figures 6 and 7) showed elevated that TNF- α (Figure 6B, $P = 0.002$), IL-1 β (Figure 6D, $P = 0.029$) and IL-6 (Figure 6F, $P = 0.003$) were significantly reduced by DFO (Figure 6A-F). TRAP (Figure 7B, $P = 0.002$) and CTSK (Figure 7D, $P = 0.01$) staining further demonstrated that local DFO administration reduced osteoclastogenesis in the maxillary regions (Figure 7A-D).

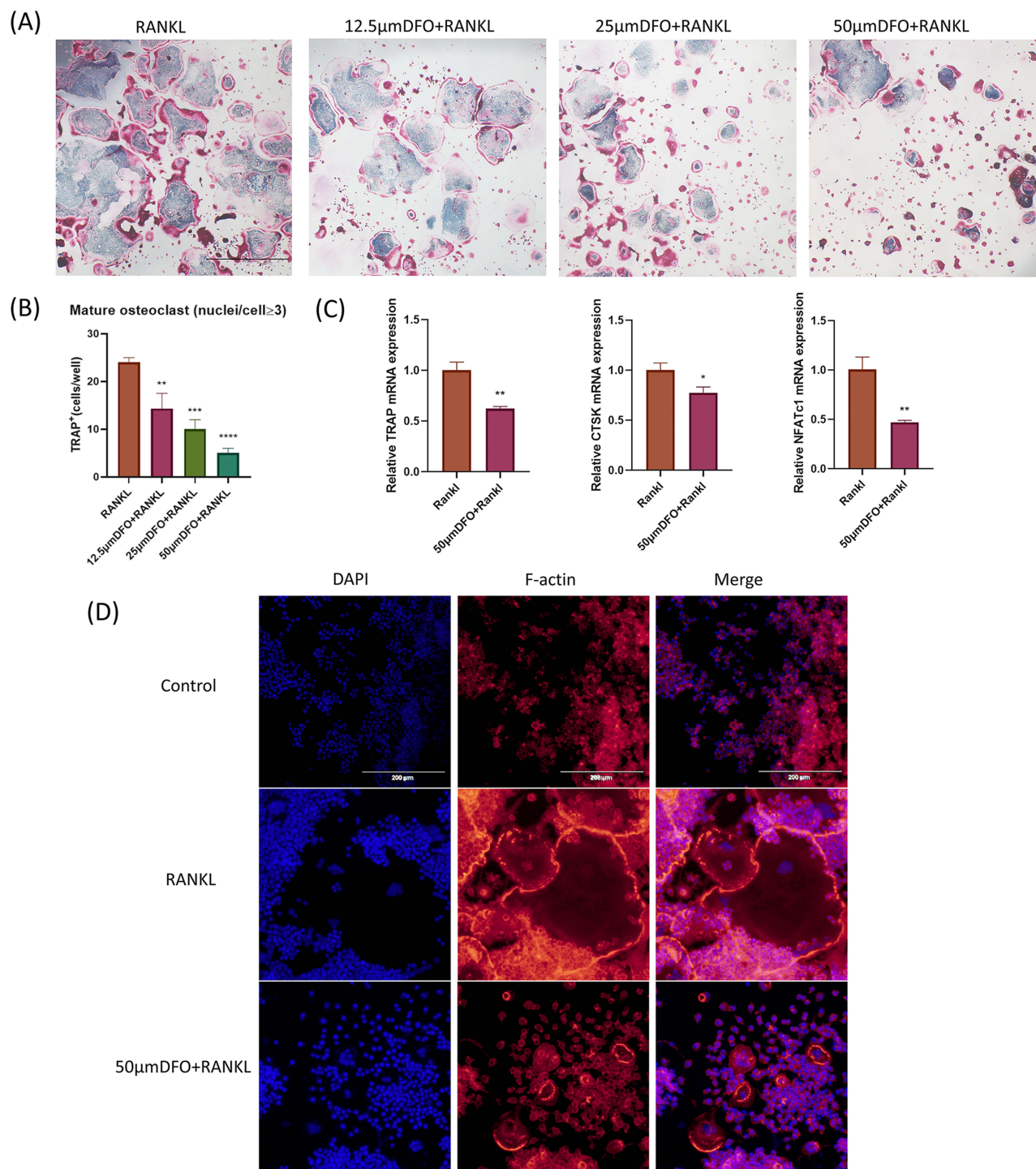


Figure 4 DFO inhibits RANKL-induced osteoclast differentiation in vitro. RAW264.7 cells were pretreated with DFO for 2 hours, followed by incubation with 50 ng/mL RANKL for 5 days. (A) TRAP staining of osteoclasts; (D) immunofluorescent staining for F-actin. Scale bar = 200 µm. TRAP-positive osteoclasts (A) were quantified, and mature osteoclast size was determined by nuclei count per osteoclast (B). (C) mRNA expression levels of TRAP, NFATc1, and CTSK were analyzed by RT-qPCR. n = 3 per group. Data are mean \pm SD; * P < 0.05, ** P < 0.01, *** P < 0.001, **** P < 0.0001.

Discussion

The study's primary focus is on investigating the efficacy of DFO as a treatment for periodontitis. The results in the rat periodontitis model demonstrate that DFO treatment significantly reduced inflammation, osteoclastogenesis and bone loss. Therefore, the first experimental hypothesis was rejected. The secondary outcome is DFO prevents the activation

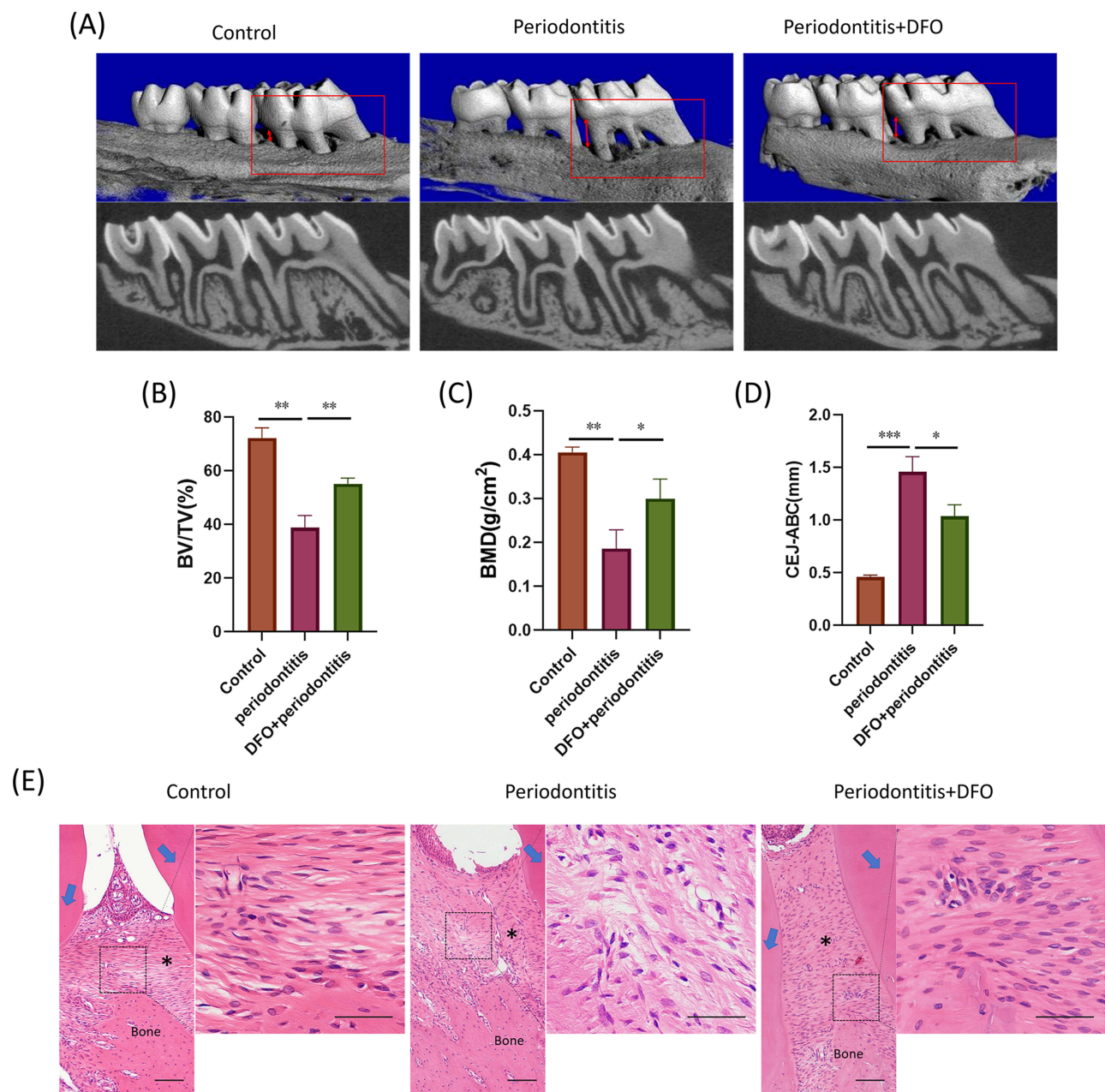


Figure 5 DFO reduces alveolar bone loss and periodontal inflammation in a rat periodontitis model. **(A)** The maxillary first molar was selected for modeling, wrapped with 0.2-mm orthodontic ligature wire (red arrow). **(B)** Representative micro-CT images of the maxillae; the red arrow indicates the distance between the cemento-enamel junction and alveolar bone crest. **(C-E)** Analysis of bone volume/tissue volume (BV/TV), bone mineral density (BMD), and distance from the enamel-cement junction to the alveolar bone crest (CEJ-ABC). **(F)** H&E-stained periodontal tissue sections; scale bar = 100 μ m. The blue arrow indicates the tooth; * represents the periodontal ligament area. n = 3 per group. Data presented as mean \pm SD; * P < 0.05, ** P < 0.01, *** P < 0.001.

and nuclear translocation of NF- κ B, a key transcription factor involved in inflammation. As a result, the second experimental hypothesis was not accepted.

A well-established *in vivo* method was used to induce periodontitis in rat models. These models consistently displayed lower BMD and BV/TV ratios, indicating alveolar bone loss following *P.g*-LPS infection.²⁰ Furthermore, the rat models had increased IL-6, TNF- α , and IL-1 β concentrations, indicating inflamed periodontal tissues. Experimental results showed that administering a local injection of DFO effectively mitigated pathological development in rat models, demonstrating DFO's therapeutic potential. Previous studies align with the anti-inflammatory effects observed with DFO.²¹ In a tooth replantation model, DFO was reported to reduce reactive oxygen species generation as

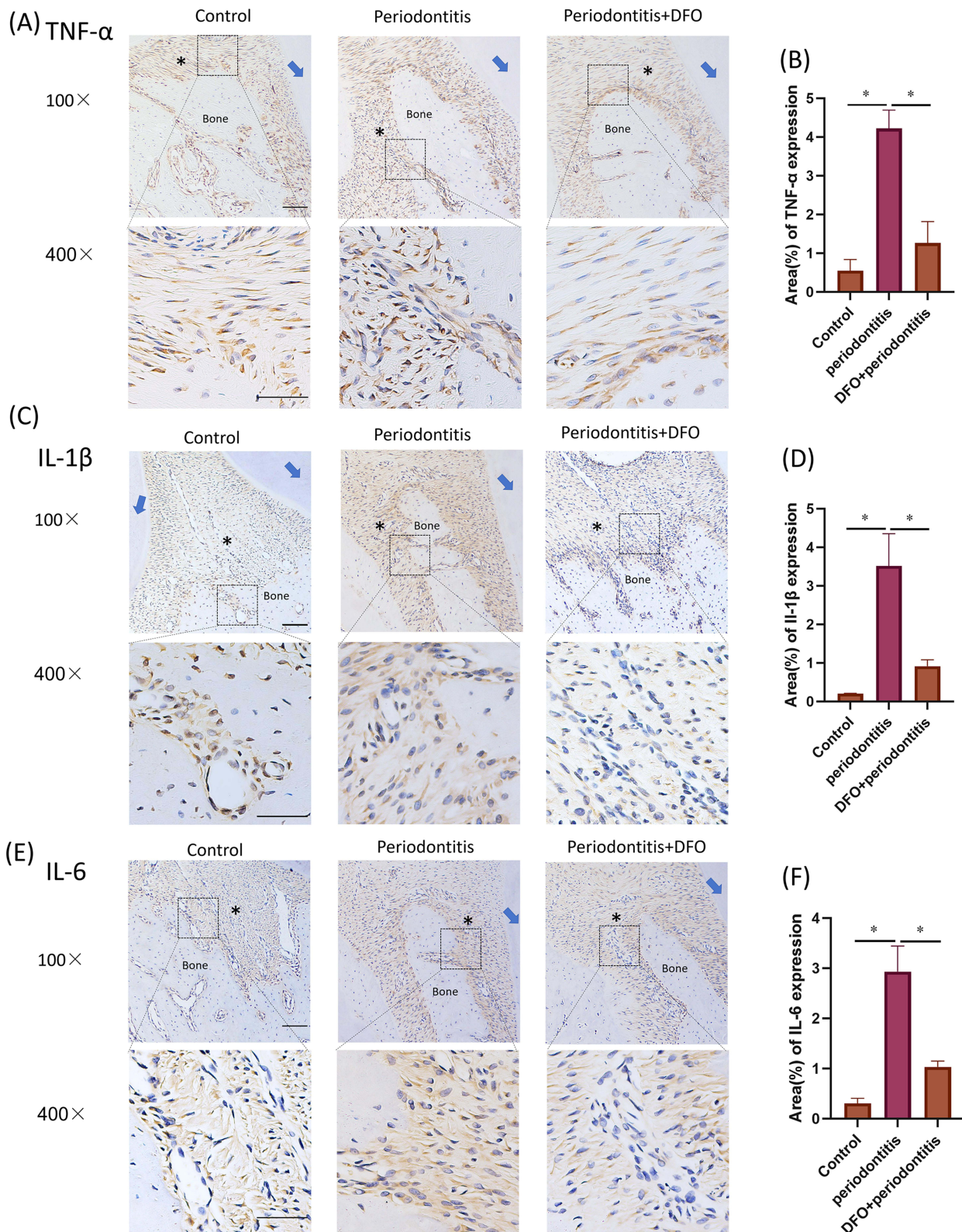


Figure 6 DFO reduces periodontal inflammation in rat periodontitis. **(A)**, **(C)**, and **(E)** Immunohistochemical staining for IL-6, IL-1 β , and TNF- α in periodontal tissues of Control, Periodontitis, and Periodontitis+DFO groups. The blue arrow indicates the tooth; * represents the periodontal ligament area; scale bar = 50 μ m. **(B)**, **(D)**, and **(F)** Quantification of immunohistochemical staining for TNF- α , IL-1 β , and IL-6 in periodontal tissue. Data presented as mean \pm SD; n = 3 per group; *P < 0.05.

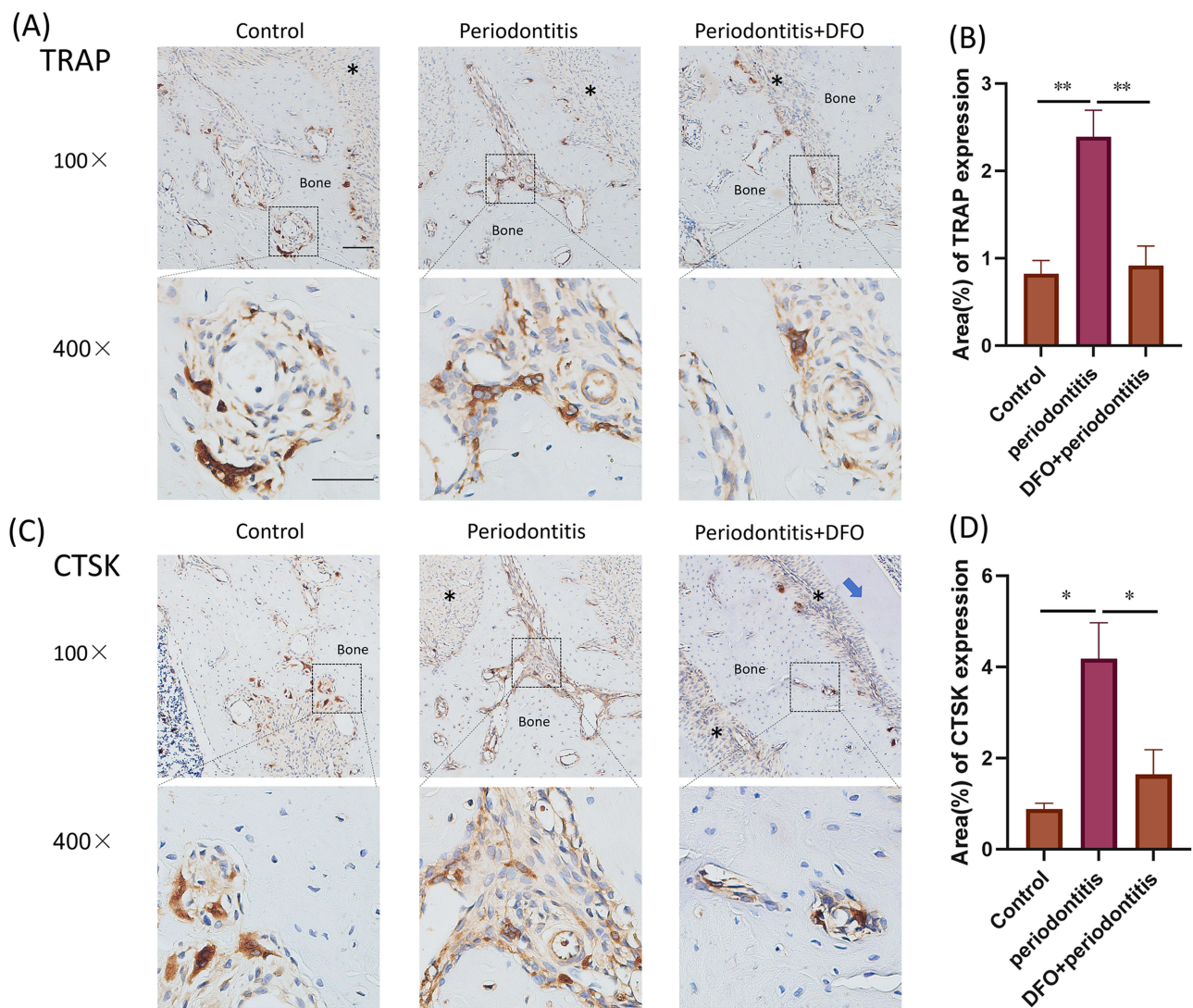


Figure 7 DFO inhibits osteoclast differentiation in the alveolar bone of rat periodontitis model. **(A)** and **(C)** Immunohistochemical staining for TRAP and CTSK in periodontal tissues of Control, Periodontitis, and Periodontitis+DFO groups. The blue arrow indicates the tooth; * represents the periodontal ligament area; scale bar = 50 μ m. **(B)** and **(D)** Quantification of TRAP and CTSK staining in periodontal tissue. Data presented as mean \pm SD; n = 3 per group. * p < 0.05, ** p < 0.01.

well as IL-1 β and IL-6 expression.²² Furthermore, culturing macrophages on hydrogels containing DFO reduced IL-6 and TNF- α production, thereby significantly altering the inflammatory response in these cells.^{23,24}

During periodontitis progression, pro-inflammatory factors and LPS may activate the classical NF- κ B axis in macrophages, triggering inflammation.²⁵ The p65 subunit of NF- κ B, an essential component of the NF- κ B transcription factor complex, facilitates the transcription of genes mediating inflammatory responses.²⁶ The inhibitor protein κ B (I κ B) interacts with NF- κ B in the cytoplasm upon stimuli like LPS binding of LPS to cell surface receptors, I κ B undergoes phosphorylation and subsequent degradation.²⁷ This process activates I κ B Kinase, which further phosphorylates and degrades I κ B α , releasing and activating NF- κ B. Once activated, NF- κ B promotes the secretion of inflammatory mediators from macrophages, intensifying the inflammatory response.²⁸ Phosphorylation of the p65 subunit is essential within this pathway. As part of the NF- κ B family, p65 binds to I κ B proteins, preventing their nuclear entry in inactive form. In response to bacterial infection or inflammatory signals, I κ B undergoes phosphorylation and degradation, facilitating NF- κ B activation. This process releases NF- κ B p65, facilitating its nuclear translocation, where it activates the transcription of key inflammation-related genes.²⁹ Our results demonstrate the regulatory effects of DFO on the NF- κ B signaling pathway. Following Pg-LPS-induced inflammation, DFO exerted anti-inflammatory effects by reducing

phosphorylation of both p65 and I κ B α in RAW264.7 cells. Furthermore, DFO reduced p65's nuclear translocation, thereby preventing activation of the NF- κ B axis.

Alveolar bone resorption is a primary manifestation of periodontitis, closely linked to inflammation driven by host factors.³⁰ In this condition, overactive osteoclasts lead to significant alveolar bone loss.³¹ TRAP is a crucial indicator of active osteoclast differentiation.³² The RANK/RANKL signaling pathway initiates osteoclasts, heavily regulated by NFATc1 expression, which promotes TRAP and CTSK production to release acid and degrade bone matrix, leading to bone loss.³³ RT-qPCR was performed to quantify CTSK, TRAP, and NFATc1 expression in RANKL-induced cells. DFO pretreatment significantly downregulated the expression of those osteoclast-related genes. Moreover, osteoclast activity depends on F-actin rings, which are important for cell morphology and function. The binding of osteoclasts to bone surfaces is facilitated by the F-actin ring structure.⁴ TRAP and F-actin staining revealed that DFO treatment reduces osteoclast numbers and alters cell morphology by affecting F-actin ring formation, suggesting that DFO modulates cytoskeletal reorganization, which impacts osteoclast differentiation and function.

In vivo, local DFO injections into periodontal sites significantly reduced inflammation, osteoclast differentiation, and alveolar bone loss. The role of PHD inhibitors in regulating the HIF pathway has highlighted their potential as targets for pharmacologic intervention in inflammatory diseases.³⁴ In a mouse colitis model, stabilizing HIF-1 α through hydroxylase inhibition and hypoxia mimicry significantly reduced inflammatory markers and disease severity.³⁵ Furthermore, PHD inhibitors partially downregulated the levels of inflammatory cytokines in human gingival fibroblasts that had been infected with *Fusobacterium nucleatum*.³⁶ In mouse periodontitis models, PHD inhibitor treatment reduced pro-inflammatory cytokines, altered anti-inflammatory IL-10 and IL-4 levels, and increased HIF-1 α -positive cells in periodontal tissue.² HIF is regulated by immunological stimuli and metabolic indicators, serving as a key mediator of both.³ The metabolic reprogramming of macrophages is dependent on HIF-1 α which inhibits oxidative phosphorylation and regulates the synthesis of transcriptional enzymes involved in glycolysis.^{8,13} Given its critical role, further investigation into inflammatory cytokines as potential HIF pathway modulators could support new therapeutic approaches for inflammatory diseases.³⁷ Overall, these findings highlight the potential of targeting the HIF signaling pathway as a treatment intervention for inflammatory diseases.

DFO has been investigated for other conditions, however its potential for periodontal treatment has been largely unexplored until now. This study showed DFO's regulatory effects on osteoclastogenesis and inflammation during periodontitis progression from vivo and vitro experiments. Our findings open up promising avenues for research and clinical application of DFO in the fight against periodontitis. While the study demonstrates DFO's efficacy in reducing bone loss, it did not fully elucidate the precise mechanisms by which DFO inhibits osteoclast differentiation. A deeper understanding of how DFO interacts with specific inflammatory pathways and influences bone remodeling processes could lead to more targeted and effective treatment strategies. Further investigation into the specific signaling pathways targeted by DFO is crucial to understand its full therapeutic potential and optimize its application in future.

Conclusion

This study provides novel evidence about the role of DFO in the treatment of periodontitis. Unlike existing therapies, DFO has the potential to not only control inflammation but also protect bones, offering a more targeted and complete approach to treating periodontitis. These preclinical findings deserve further investigation in clinical trials to assess the efficacy and safety of DFO in treating human patients.

Ethics Approval

The Animal Ethics Committee of Basic Medicine at Jilin University (No. 2022033) approved all experiments which were performed in accordance with the National Institutes' Guidelines for the Care and Use of Laboratory Animals (NIH Publications No. 8023, revised 1978).

Acknowledgments

The National Key R&D Program of China (2021YFC2400405) provided the funding to support this work. We acknowledge TopEdit LLC for the linguistic editing and proofreading during the preparation of this manuscript.

Author Contributions

All authors made a significant contribution to the work reported, whether that is in the conception, study design, execution, acquisition of data, analysis and interpretation, or in all these areas; took part in drafting, revising or critically reviewing the article; gave final approval of the version to be published; have agreed on the journal to which the article has been submitted; and agree to be accountable for all aspects of the work.

Disclosure

The authors declare that the research was conducted in the absence of any commercial or financial relationships that could be construed as a potential conflict of interest.

References

1. Cekici A, Kantarci A, Hasturk H, Van Dyke TE. Inflammatory and immune pathways in the pathogenesis of periodontal disease. *Periodontol*. 2000; 2014;64(1):57–80. doi:10.1111/prd.12002
2. Chen MH, Wang YH, Sun BJ, et al. HIF-1 α activator DMOG inhibits alveolar bone resorption in murine periodontitis by regulating macrophage polarization. *Int Immunopharmacol*. 2021;99:107901. doi:10.1016/j.intimp.2021.107901
3. Halligan DN, Murphy SJ, Taylor CT. The hypoxia-inducible factor (HIF) couples immunity with metabolism. *Semin Immunol*. 2016;28(5):469–477. doi:10.1016/j.smim.2016.09.004
4. Sun S, Yan T, Yang N, Wu J, Liu Z. Regulation of osteoclast differentiation and inflammatory signaling by TCF8 in periodontitis. *Oral Dis*. 2024;30(4):2580–2591. doi:10.1111/odi.14623
5. Nedzi-Gora M, Kowalski J, Gorska R. The immune response in periodontal tissues. *Arch Immunol Ther Exp*. 2017;65(5):421–429. doi:10.1007/s00005-017-0472-8
6. Palomaki S, Pietila M, Laitinen S, et al. HIF-1 α is upregulated in human mesenchymal stem cells. *Stem Cells*. 2013;31(9):1902–1909. doi:10.1002/stem.1435
7. Cramer T, Yamanishi Y, Clausen BE, et al. HIF-1 α is essential for myeloid cell-mediated inflammation. *Cell*. 2003;112(5):645–657. doi:10.1016/s0092-8674(03)00154-5
8. Kelly B, O'Neill LA. Metabolic reprogramming in macrophages and dendritic cells in innate immunity. *Cell Res*. 2015;25(7):771–784. doi:10.1038/cr.2015.68
9. Semenza GL. Pharmacologic targeting of hypoxia-inducible factors. *Annu Rev Pharmacol Toxicol*. 2019;59(1):379–403. doi:10.1146/annurev-pharmtox-010818-021637
10. Tchanque-Fossuo CN, Dahle SE, Buchman SR, Isseroff RR. Deferoxamine: potential novel topical therapeutic for chronic wounds. *Br J Dermatol*. 2017;176(4):1056–1059. doi:10.1111/bjd.14956
11. Velasquez J, Wray AA. *Deferoxamine*. StatPearls. 2022.
12. Keberle H. The biochemistry of desferrioxamine and its relation to iron metabolism. *Ann N Y Acad Sci*. 1964;119(2):758–768. doi:10.1111/j.1749-6632.1965.tb54077.x
13. Phelan JJ, McQuaid K, Kenny C, et al. Desferrioxamine supports metabolic function in primary human macrophages infected with mycobacterium tuberculosis. *Front Immunol*. 2020;11:836. doi:10.3389/fimmu.2020.00836
14. Manresa MC, Smith L, Casals-Diaz L, et al. Pharmacologic inhibition of hypoxia-inducible factor (HIF)-hydroxylases ameliorates allergic contact dermatitis. *Allergy*. 2019;74(4):753–766. doi:10.1111/all.13655
15. Cummins EP, Doherty GA, Taylor CT. Hydroxylases as therapeutic targets in inflammatory bowel disease. *Lab Invest*. 2013;93(4):378–383. doi:10.1038/labinvest.2013.9
16. Palazon A, Goldrath Ananda W, Nizet V, Johnson Randall S. HIF transcription factors, inflammation, and immunity. *Immunity*. 2014;41(4):518–528. doi:10.1016/j.immuni.2014.09.008
17. Cummins EP, Keogh CE, Crean D, Taylor CT. The role of HIF in immunity and inflammation. *Mol Aspects Med*. 2016;47–48:24–34. doi:10.1016/j.mam.2015.12.004
18. Zhang J, Hu W, Ding C, Yao G, Zhao H, Wu S. Deferoxamine inhibits iron-uptake stimulated osteoclast differentiation by suppressing electron transport chain and MAPKs signaling. *Toxicol Lett*. 2019;313:50–59. doi:10.1016/j.toxlet.2019.06.007
19. Zhang J, Tong D, Song H, et al. Osteoimmunity-regulating biomimetically hierarchical scaffold for augmented bone regeneration. *Adv Mater*. 2022;34(36):e2202044. doi:10.1002/adma.202202044
20. Qiao S, Li B, Cai Q, et al. Involvement of ferroptosis in *Porphyromonas gingivalis* lipopolysaccharide-stimulated periodontitis in vitro and in vivo. *Oral Dis*. 2023;29(8):3571–3582. doi:10.1111/odi.14292
21. Zhang WJ, Wei H, Frei B. The iron chelator, desferrioxamine, reduces inflammation and atherosclerotic lesion development in experimental mice. *Exp Biol Med*. 2010;235(5):633–641. doi:10.1258/ebm.2009.009229
22. Lee KE, Mo S, Lee HS, et al. Deferoxamine reduces inflammation and osteoclastogenesis in avulsed teeth. *Int J Mol Sci*. 2021;22(15). doi:10.3390/ijms22158225
23. Lombardo M, Esposito BP, Lourenco FR, Kaneko TM. The application of pharmaceutical quality by design concepts to evaluate the antioxidant and antimicrobial properties of a preservative system including desferrioxamine. *Daru*. 2020;28(2):635–646. doi:10.1007/s40199-020-00370-9
24. Dong X, Wu P, Yan L, et al. Oriented nanofibrous P(MMD-co-LA)/Deferoxamine nerve scaffold facilitates peripheral nerve regeneration by regulating macrophage phenotype and revascularization. *Biomaterials*. 2022;280:121288. doi:10.1016/j.biomaterials.2021.121288
25. He D, Fu S, Ye B, et al. Activation of HCA2 regulates microglial responses to alleviate neurodegeneration in LPS-induced in vivo and in vitro models. *J Neuroinflammation*. 2023;20(1):86. doi:10.1186/s12974-023-02762-5

26. Touil Y, Latreche-Carton C, Bouazzati HE, et al. p65/RelA NF-kappaB fragments generated by RIPK3 activity regulate tumorigenicity, cell metabolism, and stemness characteristics. *J Cell Biochem.* 2022;123(3):543–556. doi:10.1002/jcb.30198
27. Ozes ON, Mayo LD, Gustin JA, Pfeffer SR, Pfeffer LM, Donner DB. NF-kappaB activation by tumour necrosis factor requires the Akt serine-threonine kinase. *Nature.* 1999;401(6748):82–85. doi:10.1038/43466
28. Xie J, Li Q, Zhu XH, Gao Y, Zhao WH. IGF2BP1 promotes LPS-induced NFkappaB activation and pro-inflammatory cytokines production in human macrophages and monocytes. *Biochem Biophys Res Commun.* 2019;513(4):820–826. doi:10.1016/j.bbrc.2019.03.206
29. Wu Y, Chen D, Hu Y, et al. Ring finger protein 215 negatively regulates type I IFN production via blocking NF-kappaB p65 activation. *J Immunol.* 2022;209(10):2012–2021. doi:10.4049/jimmunol.2200346
30. Hajishengallis G. Immunomicrobial pathogenesis of periodontitis: keystones, pathobionts, and host response. *Trends Immunol.* 2014;35(1):3–11. doi:10.1016/j.it.2013.09.001
31. Li J, Sun Z, Lin Y, et al. Syndecan 4 contributes to osteoclast differentiation induced by RANKL through enhancing autophagy. *Int Immunopharmacol.* 2021;91:107275. doi:10.1016/j.intimp.2020.107275
32. Kirstein B, Chambers TJ, Fuller K. Secretion of tartrate-resistant acid phosphatase by osteoclasts correlates with resorptive behavior. *J Cell Biochem.* 2006;98(5):1085–1094. doi:10.1002/jcb.20835
33. Feng X, Teitelbaum SL. Osteoclasts: new Insights. *Bone Res.* 2013;1(1):11–26. doi:10.4248/BR201301003
34. Malkov MI, Lee CT, Taylor CT. Regulation of the Hypoxia-Inducible Factor (HIF) by pro-inflammatory cytokines. *Cells.* 2021;10(9):2340. doi:10.3390/cells10092340
35. Cummins EP, Seeballuck F, Keely SJ, et al. The hydroxylase inhibitor dimethylxalylglycine is protective in a murine model of colitis. *Gastroenterology.* 2008;134(1):156–165. doi:10.1053/j.gastro.2007.10.012
36. Shang L, Kang W, Li S, Ge S. Prolyl hydroxylase inhibitor DMOG suppressed inflammatory cytokine production in human gingival fibroblasts stimulated with *Fusobacterium nucleatum*. *Clin Oral Investig.* 2019;23(7):3123–3132. doi:10.1007/s00784-018-2733-2
37. Watts ER, Walmsley SR. Inflammation and hypoxia: HIF and PHD isoform selectivity. *Trends Mol Med.* 2019;25(1):33–46. doi:10.1016/j.molmed.2018.10.006

Journal of Inflammation Research

Dovepress

Publish your work in this journal

The Journal of Inflammation Research is an international, peer-reviewed open-access journal that welcomes laboratory and clinical findings on the molecular basis, cell biology and pharmacology of inflammation including original research, reviews, symposium reports, hypothesis formation and commentaries on: acute/chronic inflammation; mediators of inflammation; cellular processes; molecular mechanisms; pharmacology and novel anti-inflammatory drugs; clinical conditions involving inflammation. The manuscript management system is completely online and includes a very quick and fair peer-review system. Visit <http://www.dovepress.com/testimonials.php> to read real quotes from published authors.

Submit your manuscript here: <https://www.dovepress.com/journal-of-inflammation-research-journal>